This is an open access article published under an ACS AuthorChoice License, which permits copying and redistribution of the article or any adaptations for non-commercial purposes.

THE JOURNAL OF PHYSICAL CHEMISTRY Letters

Letter

Cite This: J. Phys. Chem. Lett. 2019, 10, 1709−1715

pubs.acs.org/JPCL

Protein Short-Time Diffusion in a Naturally Crowded Environment

Marco Grimaldo,[*,†] Hender Lopez,[†,‡,§] Christian Beck,[†,‡] Felix Roosen-Runge,[*,∥] Martine Moulin,[†] Juliette M. Devos,[†] Valerie Laux,[†] Michael Härtlein,[†] Stefano Da Vela,[‡,¶] Ralf Schweins,[†] Alessandro Mariani,[⊥] Fajun Zhang,[‡] Jean-Louis Barrat,[§] Martin Oettel,[‡] V. Trevor Forsyth,[#,†] Tilo Seydel,[*,†] and Frank Schreiber[‡]

[†]Institut Max von Laue - Paul Langevin (ILL), CS 20156, F-38042 Grenoble Cedex 9, France

[‡]Institut für Angewandte Physik, Auf der Morgenstelle 10, 72076 Tübingen, Germany

[§]LiPhy, 38402 Saint Martin d'Hères, France

[∥]Division of Physical Chemistry, Lund University, Naturvetarvägen 14, 22100 Lund, Sweden

[⊥]European Synchrotron Radiation Facility (ESRF), CS 40220, F-38042 Grenoble Cedex 9, France

[#]Faculty of Natural Sciences & Institute for Science and Technology in Medicine, Keele University, Staffordshire ST5 5BG, United Kingdom

Supporting Information

ABSTRACT: The interior of living cells is a dense and polydisperse suspension of macromolecules. Such a complex system challenges an understanding in terms of colloidal suspensions. As a fundamental test we employ neutron spectroscopy to measure the diffusion of tracer proteins (immunoglobulins) in a cell-like environment (cell lysate) with explicit control over crowding conditions. In combination with Stokesian dynamics simulation, we address protein diffusion on nanosecond time scales where hydrodynamic interactions dominate over negligible protein collisions. We successfully link the experimental results on these complex, flexible molecules with coarse-grained simulations providing a consistent understanding by colloid theories. Both experiments and simulations show that tracers in polydisperse solutions close to the effective particle radius $R_{eff} = \langle R_i^3 \rangle^{1/3}$ diffuse approximately as if the suspension was monodisperse. The simulations further show that macromolecules of sizes $R > R_{eff}$ ($R < R_{eff}$) are slowed more (less) effectively even at nanosecond time scales, which is highly relevant for a quantitative understanding of cellular processes.

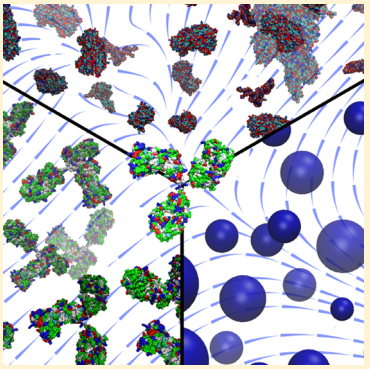

Living cells are filled with a polydisperse mixture of proteins and other macromolecules (including DNA, RNA, and polysaccharides) suspended in water at high volume fractions (typically 10−40%). The varying crowding levels of proteins in living cells may affect their mobility, folding, and stability, and thus the physical chemistry and physiology of cells.[1−3] Several experimental studies have addressed protein diffusion *in vivo*[4−9] and *in vitro*,[10−19] mostly by means of NMR, fluorescence spectroscopy, and neutron scattering, and the topic has also been the subject of several computational studies.[20−24] In general, protein diffusion was found to decrease with increasing crowding, although the details of how diffusion is modified by different cellular microenvironments are still unclear.[20]

A quantitative theoretical understanding of diffusion is generally easier in connection with *in vitro* studies which offer better control on many physical parameters such as types of crowding agents, macromolecular concentration, and temperature. Hence, they are better suited to systematic investigations regarding such parameters, although at the expense of simplifying the complex physiological environment, which is instead fully captured by *in vivo* studies. These in turn suffer from the lacking flexibility in changing specific cellular conditions. Here, we establish a framework combining both approaches with the use of tunable cell lysate. At the same time, in our simulations we go beyond standard colloidal modeling (using monodisperse crowders) and explicitly take into account the polydispersity of a cellular environment. In that way, we understand the influence of a cell-like crowded environment on the short-time diffusion of polyclonal bovine immunoglobulins (Igs), used as model nonspherical proteins, based on simple biophysical concepts.

To perform a controlled experiment under rather realistic conditions, *Escherichia coli* cells were adapted to a fully deuterated environment as previously described.[25] The cells were then lysed and the membranes were removed. Subsequently, the cell material was collected and concentrated to produce the lysate (cf. Supporting Information). Perdeuterated lysate was used as a cytosol-mimicking polydisperse crowded environment. The concentrations c_{Ig} and c_{lys} of Ig and the lysate,

Received: February 6, 2019
Accepted: March 21, 2019
Published: March 21, 2019

Downloaded via KEELE UNIV on May 16, 2019 at 10:27:32 (UTC).
See https://pubs.acs.org/sharingguidelines for options on how to legitimately share published articles.

© 2019 American Chemical Society

DOI: 10.1021/acs.jpclett.9b00345
J. Phys. Chem. Lett. 2019, 10, 1709−1715

respectively, were varied covering a total volume fraction range $6\% \lesssim \varphi \lesssim 17\%$ and ratios $0.4 \lesssim \varphi_{Ig}/\varphi \lesssim 0.8$ (φ_{Ig} is the Ig volume fraction) to systematically investigate the influence of different polydispersity. Macromolecular mass fractions of protein (82.5%), nucleic acids (14.5%), and lipids (1%) were experimentally estimated, and an additional 2% mass fraction of sugars was assumed.[26] An average partial specific volume $\nu_{lys} = 0.66$ mL/g for the macromolecular components of lysate was calculated accordingly[27,28] (cf. Supporting Information). Small angle neutron scattering (SANS),[29] as well as (ultra) small-angle X-ray scattering (USAXS/SAXS)[30] and static light scattering (SLS) were used to further characterize the lysate and qualitatively assess the batch dependence of the lysate composition, as well as to check for potential aggregation of Ig in lysate (see the Supporting Information for details). The data indicate that, as expected, the lysate contains macromolecules and assemblies having a very broad range of shapes and length scales up to several micrometers, as seen by small-angle X-ray scattering. The precise composition varied between the different batches used in this study. This polydispersity and variation of the lysate composition is important in testing the generality of the observations and the robustness of the results. It also contributes to having environments that are as realistic as possible. Solutions of the polyvalent Igs used in the present work were previously studied by Da Vela et al.,[31] who found them stable at the concentrations considered here. Our additional SANS data show that Ig aggregation upon addition of lysate is negligible in our system.

Neutron backscattering (NBS) was employed to record incoherent quasi-elastic neutron scattering (QENS). This technique has, among others, the advantage of being label-free, noninvasive, and nondestructive. In this system, NBS probes predominantly the ensemble-averaged single-particle self-correlation function of the ^{1}H atoms. The other types of atoms, including deuterium (D = ^{2}H), possess a significantly smaller neutron scattering cross section, and therefore contribute less to the total scattering intensity. In other words, only the use of heavy water (D_2O) and perdeuterated lysate sufficiently increases the contrast of the Igs of natural isotopic abundance with the background, allowing us to focus on the dynamics of the Ig tracers. Hence, neutrons are a unique probe for the determination of the self-diffusion (rotational and translational), or synonymously tracer diffusion, of the model proteins.

On the picosecond to nanosecond time scale and nanometer length scale probed by NBS, proteins typically do not diffuse sufficiently to collide with surrounding molecules, but naturally interact with the environment through hydrodynamic interactions (HI) in this regime of short-time diffusion. In addition to the experiments, we perform computer simulations providing accurate information on the diffusion of proteins in crowded environments.[22,23] Simulations were recently successfully employed to interpret and rationalize neutron scattering experiments.[32,33] Because of the time scales and the relevance of HI in our experiments, we perform simulations based on Stokesian dynamics[34,35] in which HI are considered explicitly and short-time properties can be calculated. Knowledge on the short-time diffusion as well as HI and its dependence on volume fraction is not only of fundamental intrinsic interest but also a prerequisite to quantitatively predict and correctly interpret the long-time diffusion[36−39] relevant for several biochemical processes,[36] and being strongly influenced by protein-shape effects.[40] These processes include any diffusion-limited mechanism involving two or more macromolecules such as the formation of protein complexes,[41] the binding of enzymes to substrates,[42] or protein aggregation,[43] as well as the assembly of intercellular structures such as tubulin and actin filaments, and signal transduction.[36]

To investigate the short-time self-diffusion of Ig in lysate, we employ QENS using IN16B.[44] With QENS, the scattering function $S(q,\omega)$ is recorded, where $\hbar\omega$ is the energy transfer and q is the scattering vector. A spectrum $S(q,\omega)$ of a mixture of Ig at a concentration of 67 mg/mL and lysate at 56 mg/mL at $q = 0.29$ Å^{-1} is shown in the insets of Figure 1 (red circles), after

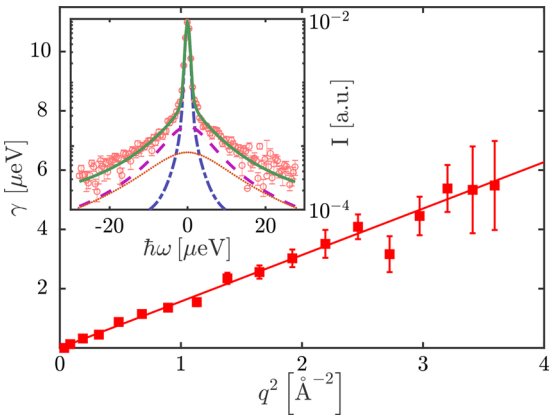

Figure 1. Example quasi-elastic neutron scattering data. Inset: scattering function $S(q,\omega)$ (red circles) of Ig at a concentration of 67 mg/mL in *E. coli* lysate at 56 mg/mL at $T = 293$K after subtraction of the lysate contribution, at $q = 0.29$Å. The points were rebinned in the plot, for clarity. The lines depict the Lorentzian functions $\mathcal{L}(\gamma(q),\omega)$ (blue dot-dashed) $\mathcal{L}(\gamma(q) + \Gamma(q),\omega)$ (magenta dashed) and $\mathcal{L}(\gamma_{D_2O}(q),\omega)$ (orange dotted) in eq 1. The green solid line superimposed on the data is the result of the complete fit using eq 1. Main figure: half-width at half-maxima γ (red squares) vs q^2. The fit $\gamma(q) = Dq^2$ (solid red line) indicates a simple Brownian diffusive behavior. The fit range is restricted to $q^2 < 1.5$ Å^{-2}.

subtraction of the empty cuvette signal[45,46] and of the lysate contribution as explained in the Supporting Information. The data can be well described by a sum of three Lorentzian functions $\mathcal{L}(\ldots,\omega)$ (green solid line, see eq 1) modeling a slow process with line broadening $\gamma(q)$ (blue dot-dashed line), a faster process with line broadening $\gamma(q) + \Gamma(q)$ (magenta dashed line), and the separately obtained solvent contribution (orange dotted line) with fixed values for both width $\gamma_{D_2O}(q)$ and intensity $\beta_{D_2O}(q)$ as explained in the Supporting Information:

$$\begin{aligned} S(q,\omega) = \mathcal{R} \otimes \{&\beta(q)[A_0(q)\,\mathcal{L}(\gamma(q),\omega) \\ &\ldots + (1 - A_0(q))\mathcal{L}(\gamma(q) + \Gamma(q),\omega)] \\ &\ldots + \beta_{D_2O}(q)\,\mathcal{L}(\gamma_{D_2O}(q),\omega)\} \end{aligned} \quad (1)$$

In eq 1, $\mathcal{R}$ represents the instrumental resolution function, $\beta(q)$, a scalar scaling factor, and $A_0(q)$ is the elastic incoherent structure factor.[47]

For the slower process, the relationship $\gamma(q) = Dq^2$ (red solid line in Figure 1) is not imposed but arises naturally from

DOI: 10.1021/acs.jpclett.9b00345
J. Phys. Chem. Lett. 2019, 10, 1709−1715

independent fits of the spectra at each q. This q^2 scaling indicates that, on the time scale ranging from tens of picoseconds to a few nanoseconds accessible by NBS, immunoglobulins undergo a simple Fickian diffusion with apparent diffusion coefficient D (including both translational D_t and rotational D_r contributions[14]), even in the presence of lysate. For most samples, the dependence $\gamma \propto q^2$ holds well on the entire q-range. However, for the samples with the lowest signal-to-noise ratio, a stronger deviation is seen for $q^2 \gtrsim 1.5\text{Å}^{-2}$, presumably because the signal from this component weakens at high q. Hence, to avoid artifacts, we restrict the fit of $\gamma(q)$ to $q^2 < 1.5\text{Å}^{-2}$ for all samples.

The apparent diffusion coefficients D obtained from samples measured at temperatures $T = 293 \pm 2\text{K}$ are plotted versus φ in Figure 2. The gray Δ symbols refer to suspensions of Ig in pure

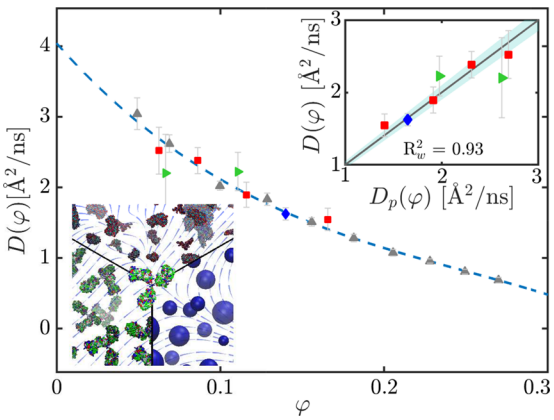

Figure 2. Experimental agreement of immunoglobulin diffusion under polydisperse and monodisperse crowding. Main figure: apparent diffusion coefficient $D(\varphi)$ as a function of the total volume fraction φ, i.e., the volume fraction of Ig and lysate combined. The symbols represent the experimental data recorded at $T = 293 \pm 2\text{K}$. Gray, pyramid symbols refer to samples of Ig in the absence of lysate, whereas other symbols and colors refer to Ig–lysate mixtures with different lysate batches (see the Supporting Information for the assignment of the batches). Finally, the dashed line depicts a polynomial fit $D_p(\varphi)$ of the diffusion of Ig in pure D_2O. Top inset: apparent diffusion coefficient $D(\varphi)$ as a function of the polynomial function $D_p(\varphi)$ for the samples in the presence of lysate (R_w^2 is the weighted coefficient of determination[49]). The shaded area depicts a ±5% deviation of $D(\varphi)$ from $D_p(\varphi)$. Bottom inset: artistic view of the two experimental systems (Ig–D_2O, bottom left, and Ig–lysate mixture, top) and of the simulations of hard-sphere suspensions (bottom right), all pointing out the importance of hydrodynamic interactions.

D_2O, in the absence of lysate. In this case, $\varphi = c_{Ig} \cdot \nu_{Ig}$, where c_{Ig} and $\nu_{Ig} = 0.739$ mL/g are the concentration and the partial specific volume of Ig,[48] respectively. The dashed line depicts a polynomial fit to that data, providing an empirical function $D_p(\varphi)$ describing the effect of self-crowding on the apparent short-time self-diffusion of Ig.

The other symbols in Figure 2, each representing one lysate batch, show D of Ig in Ig–lysate mixtures as a function of φ. In this case, $\varphi = c_{Ig} \cdot \nu_{Ig} + c_{lys} \cdot \nu_{lys}$, where c_{lys} and ν_{lys} are the concentration and the partial specific volume of the lysate components, respectively.

Overall, D in the presence and absence of lysate decreases with increasing φ in a remarkably similar manner, despite the striking difference in the crowded environment. The physical reasons for this surprising result will become clear below. The value of the reduced mean-squared deviation $\tilde{\chi}^2 \simeq 0.38$ of the data obtained in the presence of lysate from the fit $D_p(\varphi)$ for the data obtained in pure Ig solutions quantitatively supports their excellent agreement. As translational–rotational coupling is strongly protein specific,[16] we intentionally do not separate both contributions on the basis of unsupported assumptions. The good agreement of $D(\varphi) = D(D_t(\varphi), D_r(\varphi))$ for the samples with and without lysate suggests that the type of crowder is unimportant for both D_r and D_t.

This observation is further clarified in the inset of Figure 2, where D is plotted as a function of $D_p(\varphi)$: the Ig–lysate data points all lie close to the line $D = D_p(\varphi)$, with φ including the volume fraction of both Ig and the components of lysate. Within the experimental accuracy, no systematic influence on $D(\varphi)$ of the specific lysate batch is visible.

It is worth noting that the internal dynamics parameters of the function fitting the NBS spectra of Ig in the presence of lysate are found consistent with the self-crowded Ig solution (see Supporting Information). This finding suggests that the use of perdeuterated lysate may also be suitable for studies of protein internal fluctuations.

To gain further insight into the slowing down of the diffusion of Ig in lysate and the underlying physical mechanisms, we performed simulations based on Stokesian dynamics[34,35] (see Supporting Information). The method adopted only includes translational velocity–force coupling (as in ref 23); thus, only translational short-time diffusion is considered in the simulations. To mimic the biomolecular crowded environment of the experiments, the simulated lysate solutions are represented by a set of spheres of different sizes. We study two models for the *E. coli* cytoplasm, by McGuffee and Elcock[22] (ME) and by Ando and Skolnick[23] (AS), respectively. Both models have a similar average radius, 3.53 nm for the ME model and 3.64 nm for the AS model, but they represent rather different size distributions as described by their polydispersity index α defined as the standard deviation normalized by the mean of the distribution. For the ME model $\alpha = 1.05$, while for the AS model $\alpha = 0.51$ (for details regarding the size distributions see the Supporting Information). This simulation model is still a gross simplification in the description of an Ig–lysate suspension. Notably, Ig and the components of lysate are nonspherical and also have some internal flexibility. Nevertheless, with this model we capture the correct size range and size distribution which can be assumed to be the main factors influencing the hydrodynamic interactions.

Choosing two intracellular environments allows the evaluation of not only the effect of crowding on the diffusion of Ig but also the sensitivity to the polydispersity of the solution. To reproduce the experimental conditions, tracers are added to the chosen lysate, and the short-time diffusion is calculated as explained in the Supporting Information. The parameter $y_{tr} = \varphi_{tr}/\varphi$ is defined, where φ_{tr} is the volume fraction occupied by the tracers and φ the total volume fraction in the simulations, i.e., $\varphi = \varphi_{tr} + \varphi_{lys}$ with φ_{lys} the volume fraction of the lysate. In all cases the number of particles of the lysate was fixed (1001 for the ME model and 1000 for the AS model) and the size of the simulation box and the number of tracer particles was varied.

The insets of Figure 3 and Figure S7 show D_{tr}/D_0 for a tracer of the size of Ig ($R_{tr} = 5.5$ nm) as a function of D_{mono}/D_0 for the

DOI: 10.1021/acs.jpclett.9b00345
J. Phys. Chem. Lett. 2019, 10, 1709–1715

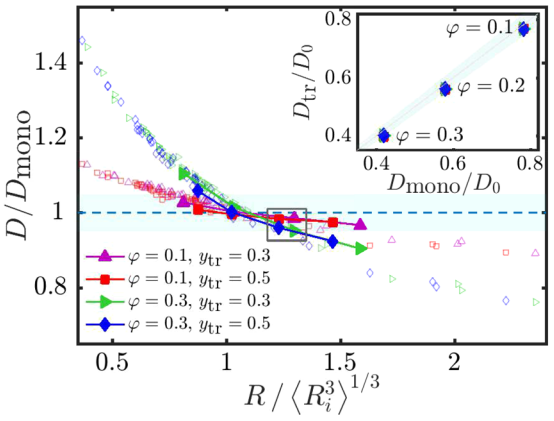

Figure 3. Simulated difference (agreement for $R \approx R_{eff}$) in particle diffusion between polydisperse and monodisperse crowding. Main figure: normalized translational diffusion coefficient D/D_{mono} of spheres with radius R, plotted against the rescaled radius R/R_{eff}. D_{mono} denotes the diffusion coefficient obtained in a monodisperse solution of spheres with radius R at similar volume fraction φ. R_{eff} is the effective radius $R_{eff} = \sqrt[3]{\langle R_i^3\rangle}$, characterizing the crowding conditions in a mixture of spheres with radii R_i. The filled symbols depict the diffusion coefficients of the *tracers* at the ratios $y_{tr} = \varphi_{tr}/\varphi$ as specified in the legend, with the tracer volume fraction φ_{tr}. In particular, the filled symbols within the gray rectangle refer to tracers with radius $R_{tr} = R_{Ig}$, as in the experiment. In this case, the deviations of the diffusion in the polydisperse environment from that in a monodisperse system are less than 5%. The empty symbols denote the diffusion coefficients of the *crowders*. These are plotted for the case $R_{tr} = R_{Ig}$. The plot refers to the ME lysate model. Inset: reduced tracer diffusion coefficient D_{tr}/D_0, where D_0 is the dilute limit diffusion coefficient, for a tracer of the size of Ig ($R = R_{Ig} = 5.5$ nm) in a crowder from the ME model as a function of the reduced diffusion coefficient D_{mono}/D_0 in the monodisperse suspension. The shaded areas (main figure and inset) depict a ±5% deviation of D_{tr} from D_{mono}.

ME and AS lysate model, respectively, where $D_0 = k_BT/6\pi\eta R$ (η being the solvent viscosity) is the dilute limit translational diffusion coefficient and D_{mono} is the translational diffusion coefficient of the tracer particles in a monodisperse solution with same total φ. D_{tr} is the translational diffusion coefficient of the tracer particles in the polydisperse mixture. In both the ME and AS model, $y_{tr} = 0.3$, 0.5, and 0.7 (nearly coinciding symbols) are presented for φ = 0.1, 0.2, and 0.3. The deviations from the monodisperse situation are small, indicating that despite the rather complex composition of the suspensions, for a tracer of the size of Ig diffusing in a cellular-like environment only small differences should be expected when compared to an equivalent system (i.e., with the same φ) composed solely of Ig under the present conditions. Additional simulations performed with different tracer radii show that the size of the tracer determines whether the normalized short-time diffusivities decrease or increase compared to the monodisperse case. Figure 3, depicts the ratio D_{tr}/D_{mono} for different φ and y_{tr} versus the normalized tracer radius (filled symbols). The normalization of the tracer radius by $R_{eff} = \sqrt[3]{\langle R_i^3\rangle}$ (angle brackets denote an average over the entire distribution of spheres in the model) is based on diffusion theory of colloids.[50] The leading order hydrodynamic interactions for the translational self-diffusion between two classes of spheres A (radius R_A) and B (radius R_B) is given by[50]

$$D_{A0} - D_A \propto R_B{}^3 R_A \int_0^\infty \mathrm{d}r\, g_{AB}(r)/r^2 \qquad (2)$$

Therein, D_A is the translational diffusion coefficient of a sphere of class A at finite concentration and D_{A0} is its dilute limit. Thus, neglecting the effects encoded in the partial radial distribution function $g_{AB}(r)$ and higher-order lubrication effects, a rough measure for the effective radius of a polydisperse crowder solution would be based on the average of $R_B{}^3$ for all particles classes B, i.e., R_{eff}. Accordingly, a tracer of radius $R_{tr} \approx R_{eff}$ is expected to behave similarly to the monodisperse situation. Indeed, $D_{tr}/D_{mono} \approx 1$ for tracer radii around R_{eff} for all compositions, indicating diffusion in polydisperse solutions comparable to monodisperse solutions. For smaller and for larger tracer radii, the deviation $|D_{tr}/D_{mono} - 1|$ becomes larger. The same trend is observed for the spheres composing the model lysate (empty symbols in Figure 3), the smallest spheres being more strongly affected by the polydispersity than the large ones. Furthermore, it is noted that increasing the level of crowding results in larger deviations from the monodisperse case for particles of radius larger or smaller than R_{eff}. Similar results are also obtained for the AS model (Figure S7) showing that despite the difference in the polydispersity between both lysate models, as indicated by their α values, the observed trend is not affected.

When comparing the hydrodynamic radius of Ig, R_{Ig}, to the effective radii of the lysate−protein solutions, a ratio $R_{Ig}/R_{eff} \approx 0.9 - 1.3$ is obtained, which explains the observed insensitivity to polydispersity. The simulation clearly indicates that this experimental observation is limited to proteins of a rather large size. We remark that, in the absence of the tracers, $R_{eff} \simeq 3.95$ nm and 4.68 nm, for the ME and AS distributions, respectively. In both cases, R_{eff} is significantly larger than the mean radius of the distribution, and thus most macromolecules (ME ≈92%, AS ≈87%) are expected to diffuse faster in the cytoplasm than in a monodisperse system at the same volume fraction. However, e.g., ribosomes as a very abundant macromolecular complex in the cytosol[51] with a radius around 10 nm would be strongly slowed down compared to monodisperse conditions. The simulation results suggest that polydispersity in the cytosol causes the general trend to slow down larger macromolecules more strongly than smaller particles via hydrodynamic interactions already at nanosecond time scales, before proteins collide. This slowing down will then unavoidably affect also molecular mobilities and escape rates for the descriptions of long-time processes. Our results imply that the dynamical heterogeneity of a structurally heterogeneous system is significantly increased by crowding, which obviously has numerous implications for the understanding of the cellular machinery. We remark that our results based on the hydrodynamic interactions in the diffusive short-time limit cannot be directly transferred to the long-time regime, where other factors such as direct potential interactions might be comparable to the effect of polydispersity.

In summary, to gain a better understanding of the effect of macromolecular crowding on the picosecond to nanosecond protein self-dynamics under controlled but realistic conditions, a quasi-elastic neutron backscattering experiment was designed. In this study, the tracer diffusion of proteins of natural isotopic abundance in perdeuterated lysate mimicking the cellular environment was followed. In this way, we benefit from the

DOI: 10.1021/acs.jpclett.9b00345
J. Phys. Chem. Lett. 2019, 10, 1709−1715

incoherent contrast between tracer proteins naturally containing hydrogen and deuterated lysate and solvent (D_2O). In order to systematically investigate the influence of polydispersity on short-time diffusion, we vary the concentration of lysate and of the nonspherical model protein Ig and find its diffusive motion on a nanosecond time scale and nanometer length scale to be determined, within the current accuracy of the experiment, only by the volume fraction φ occupied by all macromolecules present (in this case $\varphi = \varphi_{Ig} + \varphi_{lys}$). This observation is further corroborated by the fact that the different lysate batches with slightly different compositions lead to consistent results. Our experiments demonstrate the suitability of deuterated lysate as a tunable biomimicking crowding agent for neutron scattering experiments, which opens various opportunities for future systematic studies of the impact of a natural environment on protein global and internal dynamics.

The experimental results strengthen a conceptual connection of complex biological systems to quantitative accounts of statistical physics of colloids and coarse-grained simulations. We find that, for a crowder composition as in a living cell, the diffusion of tracers with a radius close to the ensemble effective radius $R_{eff} = \sqrt[3]{\langle R_i^3 \rangle}$ is similar to that for a monodisperse system and weakly dependent on the tracer size. In contrast, for tracer radii differing significantly from R_{eff}, noticeable deviations are observed. The good qualitative agreement between experiments and simulations points to the major role of hydrodynamic interactions in determining the short-time protein diffusion and shows that biophysical modeling based on colloid theory is capable of describing the macromolecular diffusion even in the more complex cellular environment. This outcome also confirms the generality of coarse-grained molecular dynamics simulations and allows us to design simplified simulation setups for macromolecules in the cytosol.

Understanding how simple systems are slowed down by HI is essential to estimate the protein mobilities in different cellular compartments and hence determine the time needed for a protein to come into contact with another protein, which is highly relevant for docking reactions and ligand transport. Our result that in a polydisperse system small proteins are slowed down less and larger particles more than in a monodisperse suspension is essential information for the understanding of the cellular physical chemistry and reaction pathways. In addition this result is also relevant to the kinetics of the in-cell assembly of large structures.

■ ASSOCIATED CONTENT

Supporting Information

The Supporting Information is available free of charge on the ACS Publications website at DOI: 10.1021/acs.jpclett.9b00345.

Materials and methods and the following figures and tables: Figure S1, example spectra of pure lysate; Figure S2, comparison of spectra from pure lysate as well as mixtures; Figure S3, width of the Lorentzian function as a function q^2 for the different samples as well as example fits; Figure S4, influence of lysate subtraction on the diffusion coefficient rescaling the lysate spectra; Figure S5, influence of lysate subtraction on the diffusion coefficient interpolating between two different lysate spectra; Figure S6, fit parameters for the internal protein dynamics; Figure S7, fit results after direct subtraction of the empty cylinder (without Paalman–Pings corrections); Figure S8, broadening Γ associated with internal dynamics as a function of q^2; Figure S9, comparison of SAXS, USAXS, and SLS intensity profiles $I(q)$ of lysate from different batches; Figure S10, SANS scattering function of some mixtures of Ig and lysate; Figure S11, size distributions of the model cytoplasms by McGuffee and Elcock[22] and by Ando and Skolnick[23] used in the present study; Figure S12, diffusion coefficient D of spheres with radius R in the Ig–lysate mixture (AS lysate model[23]) normalized by the diffusion coefficient D_{mono} of spheres of the same size in a monodisperse solution as a function of R normalized by the effective radius $R_{eff} = \langle R_i^3 \rangle^{1/3}$; Table S1, estimated lysate composition (mass fraction); Table S2, composition of the lysate ME model; Table S3, composition of the lysate AS model (PDF)

■ AUTHOR INFORMATION

Corresponding Authors

*M.G. (grimaldo@ill.eu).
*F.R.-R. (felix.roosen-runge@fkem1.lu.se).
*T.S. (seydel@ill.eu).

ORCID

Marco Grimaldo: 0000-0002-3772-7137
Hender Lopez: 0000-0003-1083-6234
Christian Beck: 0000-0001-7214-3447
Felix Roosen-Runge: 0000-0001-5106-4360
Stefano Da Vela: 0000-0002-1700-4759
Fajun Zhang: 0000-0001-7639-8594
Tilo Seydel: 0000-0001-9630-1630
Frank Schreiber: 0000-0003-3659-6718

Present Address

¶European Molecular Biology Laboratory (EMBL) Hamburg, Notkestr. 85, 22607 Hamburg, Germany.

Notes

The authors declare no competing financial interest.
The data are avaliable at doi.ill.fr/10.5291/ILL-DATA.9-13-477, doi.ill.fr/10.5291/ILL-DATA.8-04-759, doi.ill.fr/10.5291/ILL-DATA.-04-774, doi.ill.fr/10.5291/ILL-DATA.9-13-620, doi.ill.fr/10.5291/ILL-DATA.-03-891.

■ ACKNOWLEDGMENTS

We acknowledge support by the Partnership for Soft Condensed Matter (PSCM). We thank M. Braun, O. Matsarskaia, and B. Sohmen for help during the experiments, as well as M. Hennig and V. Glenisson for discussion. We acknowledge financial support from the Deutsche Forschungsgemeinschaft (DFG 316738961) and the Agence Nationale de la Recherche (ANR-16-CE92-0009, ImmunoglobulinCrowding). This work was carried out using the laboratory facilities of ILL's Life Sciences group initially funded through EPSRC awards to VTF (grants EP/C015452/1, GR/R99393/01) for creation of the Deuteration Laboratory (D-Lab). F.R.-R. acknowledges the Knut and Alice Wallenberg Foundation (project grant KAW 2014.0052).

■ REFERENCES

(1) van den Berg, J.; Boersma, A. J.; Poolman, B. Microorganisms Maintain Crowding Homeostasis. *Nat. Rev. Microbiol.* **2017**, *15*, 309–318.
(2) Rivas, G.; Minton, A. P. Macromolecular Crowding in vitro, in vivo, and in between. *Trends Biochem. Sci.* **2016**, *41*, 970–981.

DOI: 10.1021/acs.jpclett.9b00345
J. Phys. Chem. Lett. 2019, 10, 1709–1715

(3) Ellis, R. Macromolecular Crowding: An Important but Neglected Aspect of the Intracellular Environment. *Curr. Opin. Struct. Biol.* **2001**, *11*, 114−119.
(4) Mamontov, E. Microscopic Diffusion Processes Measured in Living Planarians. *Sci. Rep.* **2018**, *8*, 4190.
(5) Jasnin, M.; Moulin, M.; Haertlein, M.; Zaccai, G.; Tehei, M. *In Vivo* Measurement of Internal and Global Macromolecular Motions in Escherichia Coli. *Biophys. J.* **2008**, *95*, 857−864.
(6) Diekmann, S.; Hoischen, C. Biomolecular Dynamics and Binding Studies in the Living Cell. *Phys. Life Rev.* **2014**, *11*, 1−30.
(7) Freedberg, D. I.; Selenko, P. Live Cell NMR. *Annu. Rev. Biophys.* **2014**, *43*, 171−192.
(8) Longeville, S.; Stingaciu, L.-R. Hemoglobin Diffusion and the Dynamics of Oxygen Capture by Red Blood Cells. *Sci. Rep.* **2017**, *7*, 10448.
(9) Anunciado, D. B.; Nyugen, V. P.; Hurst, G. B.; Doktycz, M. J.; Urban, V.; Langan, P.; Mamontov, E.; O'Neill, H. In vivo Protein Dynamics on the Nanometer Length Scale and Nanosecond Time Scale. *J. Phys. Chem. Lett.* **2017**, *8*, 1899−1904.
(10) Wang, Y.; Li, C.; Pielak, G. J. Effects of Proteins on Protein Diffusion. *J. Am. Chem. Soc.* **2010**, *132*, 9392−9397.
(11) Latham, M. P.; Kay, L. E. Is Buffer a Good Proxy for a Crowded Cell-Like Environment? A Comparative NMR Study of Calmodulin Side-Chain Dynamics in Buffer and E. Coli Lysate. *PLoS One* **2012**, *7*, e48226.
(12) Le Coeur, C.; Longeville, S. Microscopic Protein Diffusion at High Concentration by Neutron Spin-Echo Spectroscopy. *Chem. Phys.* **2008**, *345*, 298−304.
(13) Gupta, S.; Biehl, R.; Sill, C.; Allgaier, J.; Sharp, M.; Ohl, M.; Richter, D. Protein Entrapment in Polymeric Mesh: Diffusion in Crowded Environment with Fast Process on Short Scales. *Macromolecules* **2016**, *49*, 1941−1949.
(14) Roosen-Runge, F.; Hennig, M.; Zhang, F.; Jacobs, R. M. J.; Sztucki, M.; Schober, H.; Seydel, T.; Schreiber, F. Protein Self-Diffusion in Crowded Solutions. *Proc. Natl. Acad. Sci. U. S. A.* **2011**, *108*, 11815−11820.
(15) Grimaldo, M.; Roosen-Runge, F.; Zhang, F.; Seydel, T.; Schreiber, F. Diffusion and Dynamics of γ-Globulin in Crowded Aqueous Solutions. *J. Phys. Chem. B* **2014**, *118*, 7203−7209.
(16) Roos, M.; Ott, M.; Hofmann, M.; Link, S.; Rössler, E.; Balbach, J.; Krushelnitsky, A.; Saalwächter, K. Coupling and Decoupling of Rotational and Translational Diffusion of Proteins under Crowding Conditions. *J. Am. Chem. Soc.* **2016**, *138*, 10365−10372.
(17) Stadler, A. M.; Demmel, F.; Ollivier, J.; Seydel, T. Picosecond to Nanosecond Dynamics Provide a Source of Conformational Entropy for Protein Folding. *Phys. Chem. Chem. Phys.* **2016**, *18*, 21527−21538.
(18) Braun, M. K.; Grimaldo, M.; Roosen-Runge, F.; Hoffmann, I.; Czakkel, O.; Sztucki, M.; Zhang, F.; Schreiber, F.; Seydel, T. Crowding-Controlled Cluster Size in Concentrated Aqueous Protein Solutions: Structure, Self-and Collective Diffusion. *J. Phys. Chem. Lett.* **2017**, *8*, 2590−2596.
(19) Zhang, Z.; Liu, Y. Recent Progresses of Understanding the Viscosity of Concentrated Protein Solutions. *Curr. Opin. Chem. Eng.* **2017**, *16*, 48−55.
(20) Feig, M.; Yu, I.; Wang, P.-h.; Nawrocki, G.; Sugita, Y. Crowding in Cellular Environments at an Atomistic Level from Computer Simulations. *J. Phys. Chem. B* **2017**, *121*, 8009−8025.
(21) Myung, J. S.; Roosen-Runge, F.; Winkler, R. G.; Gompper, G.; Schurtenberger, P.; Stradner, A. Weak Shape Anisotropy Leads to a Nonmonotonic Contribution to Crowding, Impacting Protein Dynamics under Physiologically Relevant Conditions. *J. Phys. Chem. B* **2018**, *122*, 12396−12402.
(22) McGuffee, S. R.; Elcock, A. H. Diffusion, Crowding & Protein Stability in a Dynamic Molecular Model of the Bacterial Cytoplasm. *PLoS Comput. Biol.* **2010**, *6*, e1000694.
(23) Ando, T.; Skolnick, J. Crowding and Hydrodynamic Interactions Likely Dominate in vivo Macromolecular Motion. *Proc. Natl. Acad. Sci. U. S. A.* **2010**, *107*, 18457−18462.
(24) Dix, J. A.; Verkman, A. Crowding Effects on Diffusion in Solutions and Cells. *Annu. Rev. Biophys.* **2008**, *37*, 247−263.
(25) Haertlein, M.; Moulin, M.; Devos, J. M.; Laux, V.; Dunne, O.; Forsyth, V. T. *Methods in enzymology*; Elsevier, 2016; Vol. 566; pp 113−157.
(26) Alberts, B.; Johnson, A.; Lewis, J.; Walter, P.; Raff, M.; Roberts, K. *Molecular Biology of the Cell 4th ed.: International Student ed.*; Routledge, 2002.
(27) Durchschlag, H. *Thermodynamic Data for Biochemistry and Biotechnology*; Springer, 1986; pp 45−128.
(28) Von Stockar, U.; Liu, J.-S. Does Microbial Life Always Feed on Negative Entropy? Thermodynamic Analysis of Microbial Growth. *Biochim. Biophys. Acta, Bioenerg.* **1999**, *1412*, 191−211.
(29) Lindner, P.; Schweins, R. The D11 Small-Angle Scattering Instrument: A New Benchmark for SANS. *Neutron News* **2010**, *21*, 15−18.
(30) Narayanan, T.; Sztucki, M.; Van Vaerenbergh, P.; Léonardon, J.; Gorini, J.; Claustre, L.; Sever, F.; Morse, J.; Boesecke, P. A Multipurpose Instrument for Time-Resolved Ultra-Small-Angle and Coherent X-Ray Scattering. *J. Appl. Crystallogr.* **2018**, *51*, 1511−1524.
(31) Da Vela, S.; Roosen-Runge, F.; Skoda, M. W.; Jacobs, R. M.; Seydel, T.; Frielinghaus, H.; Sztucki, M.; Schweins, R.; Zhang, F.; Schreiber, F. Effective Interactions and Colloidal Stability of Bovine γ-Globulin in Solution. *J. Phys. Chem. B* **2017**, *121*, 5759−5769.
(32) Bucciarelli, S.; Myung, J. S.; Farago, B.; Das, S.; Vliegenthart, G. A.; Holderer, O.; Winkler, R. G.; Schurtenberger, P.; Gompper, G.; Stradner, A. Dramatic Influence of Patchy Attractions on Short-Time Protein Diffusion under Crowded Conditions. *Sci. Adv.* **2016**, *2*, e1601432.
(33) Wang, G.; Varga, Z.; Hofmann, J.; Zarraga, I. E.; Swan, J. W. Structure and Relaxation in Solutions of Monoclonal Antibodies. *J. Phys. Chem. B* **2018**, *122*, 2867−2880.
(34) Brady, J. F.; Bossis, G. Stokesian Dynamics. *Annu. Rev. Fluid Mech.* **1988**, *20*, 111−157.
(35) Phillips, R. J.; Brady, J. F.; Bossis, G. Hydrodynamic Transport Properties of Hard-Sphere Dispersions. I. Suspensions of Freely Mobile Particles. *Phys. Fluids* **1988**, *31*, 3462−3472.
(36) Skolnick, J. Perspective: On the Importance of Hydrodynamic Interactions in the Subcellular Dynamics of Macromolecules. *J. Chem. Phys.* **2016**, *145*, 100901.
(37) Verberg, R.; de Schepper, I.; Cohen, E. Diffusion of Concentrated Neutral Hard-Sphere Colloidal Suspensions. *Phys. Rev. E: Stat. Phys., Plasmas, Fluids, Relat. Interdiscip. Top.* **2000**, *61*, 2967−2976.
(38) Banchio, A. J.; Nägele, G.; Bergenholtz, J. Collective Diffusion, Self-Diffusion and Freezing Criteria of Colloidal Suspensions. *J. Chem. Phys.* **2000**, *113*, 3381−3396.
(39) Medina-Noyola, M. Long-Time Self-Diffusion in Concentrated Colloidal Dispersions. *Phys. Rev. Lett.* **1988**, *60*, 2705−2708.
(40) Balbo, J.; Mereghetti, P.; Herten, D.-P.; Wade, R. The Shape of Protein Crowders is a Major Determinant of Protein Diffusion. *Biophys. J.* **2013**, *104*, 1576−1584.
(41) Plattner, N.; Doerr, S.; De Fabritiis, G.; Noé, F. Complete Protein−Protein Association Kinetics in Atomic Detail Revealed by Molecular Dynamics Simulations and Markov Modelling. *Nat. Chem.* **2017**, *9*, 1005−1011.
(42) Korennykh, A. V.; Plantinga, M. J.; Correll, C. C.; Piccirilli, J. A. Linkage between Substrate Recognition and Catalysis during Cleavage of Sarcin/Ricin Loop RNA by Restrictocin. *Biochemistry* **2007**, *46*, 12744−12756.
(43) Reynolds, N. P.; Adamcik, J.; Berryman, J. T.; Handschin, S.; Zanjani, A. A. H.; Li, W.; Liu, K.; Zhang, A.; Mezzenga, R. Competition Between Crystal and Fibril Formation in Molecular Mutations of Amyloidogenic Peptides. *Nat. Commun.* **2017**, *8*, 1338.
(44) Frick, B.; Mamontov, E.; Eijck, L. V.; Seydel, T. Recent Backscattering Instrument Developments at the ILL and SNS. *Z. Phys. Chem.* **2010**, *224*, 33−60.

DOI: 10.1021/acs.jpclett.9b00345
J. Phys. Chem. Lett. 2019, 10, 1709−1715

(45) Paalman, H.; Pings, C. Numerical Evaluation of X-Ray Absorption Factors for Cylindrical Samples and Annular Sample Cells. *J. Appl. Phys.* **1962**, *33*, 2635−2639.
(46) Chelton, E.; Jones, A.; Walker, R. The Chemical Composition of the Nucleic Acids and the Proteins of Some Mycoplasma Strains. *J. Gen. Microbiol.* **1968**, *50*, 305−312.
(47) Grimaldo, M.; Roosen-Runge, F.; Jalarvo, N.; Zamponi, M.; Zanini, F.; Hennig, M.; Zhang, F.; Schreiber, F.; Seydel, T. High-Resolution Neutron Spectroscopy on Protein Solution Samples. *EPJ Web Conf.* **2015**, *83*, 02005.
(48) Jøssang, T.; Feder, J.; Rosenqvist, E. Photon Correlation Spectroscopy of Human IgG. *J. Protein Chem.* **1988**, *7*, 165−171.
(49) Willett, J. B.; Singer, J. D. Another Cautionary Note About R 2: Its Use in Weighted Least-Squares Regression Analysis. *Am. Stat.* **1988**, *42*, 236−238.
(50) Nägele, G. On the Dynamics and Structure of Charge-Stabilized Suspensions. *Phys. Rep.* **1996**, *272*, 215−372.
(51) Ishihama, Y.; Schmidt, T.; Rappsilber, J.; Mann, M.; Hartl, F. U.; Kerner, M. J.; Frishman, D. q. *BMC Genomics* **2008**, *9*, 102−1−17.

DOI: 10.1021/acs.jpclett.9b00345
J. Phys. Chem. Lett. 2019, 10, 1709−1715